

HR-NAS: Searching Efficient High-Resolution Neural Architectures with Lightweight Transformers

Mingyu Ding^{1*} XiaoChen Lian² Linjie Yang² Peng Wang² XiaoJie Jin² Zhiwu Lu³ Ping Luo¹

¹The University of Hong Kong ²Bytedance Inc.

³Gaoling School of Artificial Intelligence, Renmin University of China

{myding, pluo}@cs.hku.hk

luzhiwu@ruc.edu.cn

{xiaochen.lian, linjie.yang, peng.wang, jinxiaojie}@bytedance.com

Abstract

High-resolution representations (HR) are essential for dense prediction tasks such as segmentation, detection, and pose estimation. Learning HR representations is typically ignored in previous Neural Architecture Search (NAS) methods that focus on image classification. This work proposes a novel NAS method, called HR-NAS, which is able to find efficient and accurate networks for different tasks, by effectively encoding multiscale contextual information while maintaining high-resolution representations. In HR-NAS, we renovate the NAS search space as well as its searching strategy. To better encode multiscale image contexts in the search space of HR-NAS, we first carefully design a lightweight transformer, whose computational complexity can be dynamically changed with respect to different objective functions and computation budgets. To maintain high-resolution representations of the learned networks, HR-NAS adopts a multi-branch architecture that provides convolutional encoding of multiple feature resolutions, inspired by HRNet [76]. Last, we proposed an efficient fine-grained search strategy to train HR-NAS, which effectively explores the search space, and finds optimal architectures given various tasks and computation resources. As shown in Fig. 1 (a), HR-NAS is capable of achieving state-of-the-art trade-offs between performance and FLOPs for three dense prediction tasks and an image classification task, given only small computational budgets. For example, HR-NAS surpasses SqueezeNAS [66] that is specially designed for semantic segmentation while improving efficiency by 45.9%. Code is available at <https://github.com/dingmyu/HR-NAS>.

1. Introduction

Neural architecture search (NAS) has achieved remarkable success in automatically designing efficient models for image classification [79, 46, 50, 56, 6, 82, 5, 67, 96, 29].

*This work was done as a part of internship at Bytedance AI Lab US.

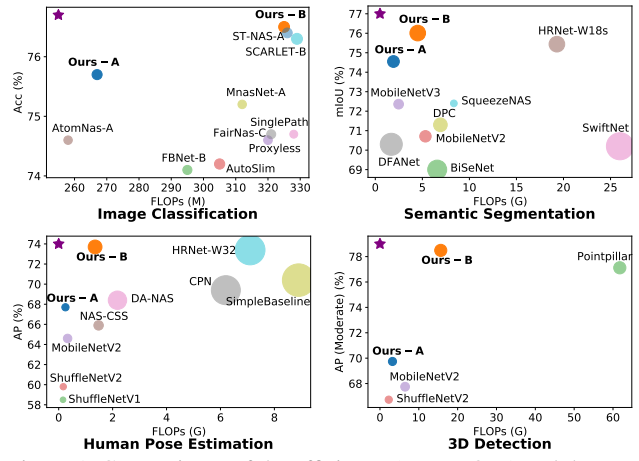


Figure 1. Comparisons of the efficiency (*i.e.*, FLOPs) and the performance (*e.g.*, Acc, mIoU, AP) on 4 computer vision tasks, *i.e.*, classification (ImageNet), segmentation (CityScapes), pose estimation (COCO), and 3D detection (KITTI), between the proposed approach and existing SoTA methods. Each method is represented by a circle, whose size represents the number of parameters. ★ represents the optimal model with both high performance and low FLOPs. Our approach achieves superior performance under similar FLOPs compared to its counterparts on all four benchmarks.

NAS has also been applied to improve the efficiency of models for dense prediction tasks such as semantic segmentation [66, 8] and pose estimation [20]. However, existing NAS methods for dense prediction either directly extend the search space designed for image classification [20, 47], only search for a feature aggregation head [57, 8], organizing network cells in a chain-like single-branch manner [49, 66]. This lack of consideration to the specificity of dense prediction hinders the performance advancement of NAS methods compared to the best hand-crafted models [76, 24].

In principle, dense prediction tasks require the integrity of the global context and the high-resolution (HR) representation; the former is critical to clarify ambiguous local features [91] at each pixel, and the latter is useful for the accu-

rate prediction of fine details [42], such as semantic boundaries and keypoint locations. However, these two aspects, especially the HR representations, have not got enough attention in existing NAS algorithms for classification. The straightforward strategy to implement the principle is manually combining multi-scale features at the end of the network [49, 9, 44], while recent approaches [24, 76, 92] show the performance can be enhanced by putting multi-scale feature processing within the network backbone. Another observation from recent research is that multi-scale convolutional representations can not guarantee a global outlook of the image since dense prediction tasks often come with high input resolution but a network often only covers a fixed receptive field. Therefore, global attention strategies such as SENet [37] and non-local network [78] have been proposed to enrich image convolutional features. Most recently, inspired by its success in natural language processing, Transformer architectures [75, 69], which contain global attention with spatial encoding, have also shown superior results when combined with convolutional neural network for image classification [27] and object detection [7].

Motivated by the above observations, in this work, we propose a NAS algorithm, which incorporates these strategies, *i.e.* in-network multi-scale features and transformers, and enables their adaptive changing with respect to task objectives and resource constraints. In practice, it is non-trivial to put them together. Firstly, Transformer has a high computational cost that is quadratic w.r.t. image pixels and hence unfriendly to the NAS search space of efficient architectures. We solve this through a dynamic down projection strategy, yielding a lightweight and plug-and-play transformer architecture that can be combined with other convolutional neural architectures. In addition, searching a fused space of multi-scale convolution and transformers needs proper feature normalization, selection of fusion strategies and balancing. We did extensive studies to calibrate various model choices that generalize to multiple tasks.

In summary, HR-NAS works as follows. We first setup a super network, where each layer contains a multi-branch parallel module followed by a fusion module. The parallel module contains searching blocks with multiple resolutions, and the fusion module contains searching blocks of feature fusion determining how feature from different resolutions fuses. Then, based on the computational budget and the task objective, a fine-grained progressive shrinking search strategy is introduced to prune redundant channels in convolutions and queries in transformers, resulting in an efficient model that provides the best trade-off between performance and computational costs. With extensive experiments, HR-NAS achieves state-of-the-art on multiple dense prediction tasks and competitive results on image classification under highly efficient settings with a single search. Fig. 1 shows a comprehensive comparison of our proposed approach with

previous NAS approaches as well as manually designed networks on four different tasks.

Our main **contributions** are three-fold. (1) We introduce a novel lightweight and plug-and-play transformer, which is highly efficient and can be easily combined with convolutional networks for computer vision tasks. (2) We propose a well-designed multi-resolution search space containing both convolutions and transformers to model in-network multi-scale information and global contexts for dense prediction tasks. To our best knowledge, we are the first to integrate transformers in a resource-constrained NAS search space for computer vision. (3) A resource-aware search strategy allows us to customize efficient architectures for different tasks. Extensive experiments show models produced by our NAS algorithm achieve state-of-the-art on three dense prediction tasks and four widely used benchmarks with lower computational costs.

2. Related Work

Transformers. Transformer [75, 69], a model architecture relying on a self-attention mechanism to learn dependencies between input and target, is used primarily in natural language processing. Generative Pre-trained Transformer (GPT) uses language modeling as a pre-training task [61, 4]. BERT [22] improves Transformer with a masked language model and a learned positional embedding to replace the sinusoidal positional encoding [75].

Since Transformer is suitable for capturing global information and pairwise interactions, some attempts [78, 7, 27, 80] have been made to adapt it to computer vision. Non-local networks [78] proposed a self-attention architecture to capture long-range interactions which can be viewed as a simplified version of Transformer. DETR [7] formulates object detection as a set prediction problem, which is naturally modeled as a sequence prediction task by the Transformer. Visual Transformers [80] represent images as a set of visual tokens and apply a Transformer-based structure to detect relationships between visual semantic concepts for semantic segmentation. iGPT [10] uses a standard Transformer to unsupervisedly learn generative relationships of image pixels. However, since its computational complexity grows quadratically with the number of pixels, such applications of Transformers in computer vision are computationally expensive. Some approaches [64, 51, 40, 77, 14] leverage network compression techniques, such as dynamic routing and knowledge distillation, to improve the efficiency of Transformers in NLP. However, efficient Transformers are seldom explored in computer vision. In light of this, we formulate Transformer into an efficient and plug-and-play module that is seamlessly integrated into a well-designed NAS search space.

Neural Architecture Search for Efficient models. Early approaches utilize reinforcement learning [97] and evo-

lution algorithms [63, 54] to find efficient and powerful network structures. However, these methods are usually computationally expensive. To improve the efficiency of the search process, differentiable search methods such as Darts [50, 41, 83] and ProxylessNAS [6] formulate the search space as a super-graph where the probability to adopt an operator is represented by a continuous importance weight, allowing an efficient search of the architecture using gradient descent. Other approaches [3, 70, 34] utilize a random sampling approach when training the super-net and search for the best model candidate after the network converges. Inspired by the manually designed structures, [71, 36] use a search space based on MobileNetV2 [65] to search for efficient structures. Mixed convolution [73, 56] is also adopted in NAS search spaces due to its multi-scale feature modeling capability. Recently, model scaling techniques are used to expand the search space from operators to other hyper-parameters such as input resolutions, channel numbers, and layer numbers [5, 88]. In order to search for efficient models, the existing methods usually borrow efficient operators from manually designed networks, such as depthwise convolution and Inverted Residual Block [65]. To construct the search space with more powerful operators, we design a new efficient Transformer structure that can be directly inserted into existing NAS search spaces.

Neural Architecture Search for Dense Prediction. The current NAS algorithms either reuse search spaces for image classification or only search for a feature aggregation head for dense prediction tasks. A single branch supernet structure is usually utilized for dense prediction tasks such as semantic segmentation [66, 49, 47], object detection [28, 13, 31], and human pose estimation [20]. Structures of feature aggregation head are also discovered using NAS algorithms for semantic segmentation [8, 57]. Recent explorations [32, 92] aim to find an optimal network layout in a hierarchical multi-scale search space. However, their search spaces use fixed width of layers which result in computationally heavy models. In contrast, we propose a multi-branch search space where each branch specializes for a typical feature resolution. The same search space can be directly used for various dense prediction tasks that have different preferences on the granularity of features, in which the computation budget is allocated for different resolutions through an end-to-end optimization.

3. Methodology

Our method aims to search for network structures within a multi-branch search space containing both Convolutions and Transformers with a resource-aware search strategy. In this section, we first introduce our lightweight Transformers. We then detail our multi-branch search space and how to integrate our Transformers into it. Finally, we describe the resource-aware fine-grained search strategy.

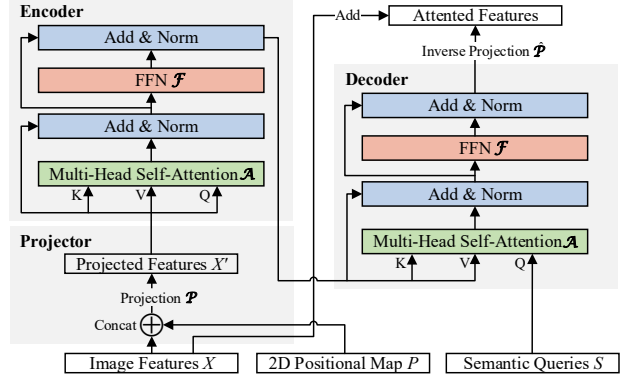


Figure 2. The architecture of our lightweight Transformer, which contains a projector, an encoder, and a decoder. It can be used plug-and-play to enhance the global context of image features.

3.1. Lightweight Transformers

The standard Transformer [75, 7] cannot be directly applied to high-resolution images and mobile scenarios, as its computational cost grows quadratically to the number of pixels. Our lightweight Transformer shown in Fig. 2, which consists of a projector, an encoder, and a decoder, is proposed to solve this issue (see Fig. 2).

Projector. To reduce the computational costs, we project the input feature $X \in \mathbb{R}^{c \times h \times w}$, together with the positional encoding, into a reduced size of $n \times s \times s$ by a projection function $\mathcal{P}(\cdot)$, where n denotes the number of queries and $s \times s$ is the reduced spatial size. Formally, the projection process can be represented by:

$$X' = \mathcal{P}(\text{Concat}(X, P)), \quad (1)$$

where Concat denotes the concatenation operator, $P \in \mathbb{R}^{d_p \times h \times w}$ is a positional encoding which compensates for the loss of spatial information during the self-attention process, and $X' \in \mathbb{R}^{n \times s^2}$ is the projected and flattened embedding. The projector \mathcal{P} first uses a point-wise convolution (with a Batch Normalization layer) to reduce the channel dimension of the feature map from $c + d_p$ to a smaller dimension n and then uses a bilinear interpolation operation to resize the spatial dimension of the feature map to $s \times s$. The positional encoding P in Eq. 1, is simply a normalized 2D positional map:

$$\begin{aligned} P[0, i, j] &= i/h, & i \in [0, h - 1] \\ P[1, i, j] &= j/w, & j \in [0, w - 1] \end{aligned} \quad (2)$$

The 2D positional map P is very efficient as it contains only 2 channels (*i.e.*, $d_p = 2$). Later in the experiments, we show that this simple encoding outperforms the sinusoidal positional encoding [75] and the learned embedding [7].

Encoder. After the projection, the original feature X is transformed into a set of n tokens X' ; each token is an s^2 -dimensional semantic embedding with positional information. X' , is then fed into our encoder as queries, keys, and

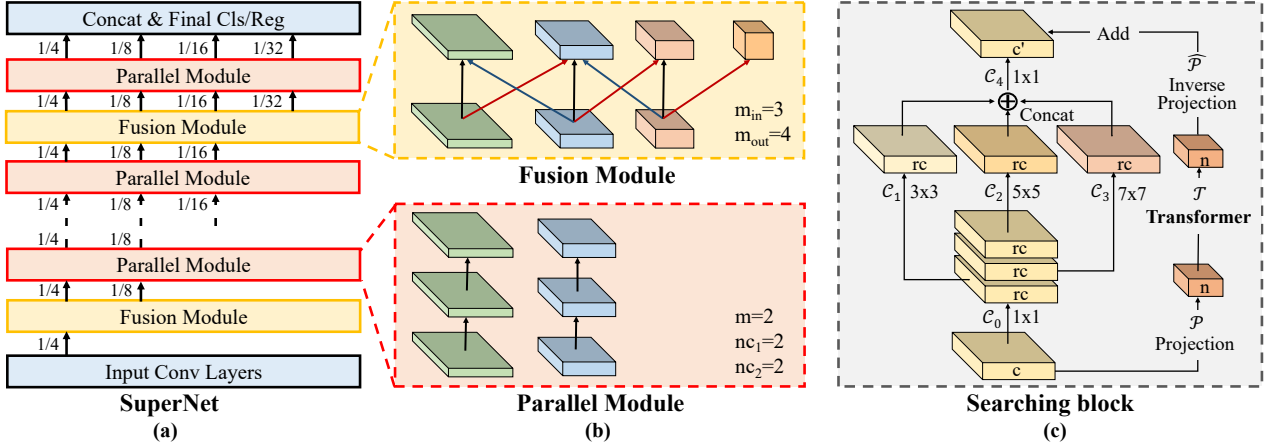


Figure 3. (a) Our multi-branch search space, which is composed of parallel modules and fusion modules alternately. “1/4, 1/8, . . .” denote the down-sampling ratios. (b) Illustration of parallel modules and fusion modules. The red, black, and blue arrows represent the reduction searching blocks, normal searching blocks, and normal searching blocks with upsampling, respectively. The cubes represent feature maps. In this example, the fusion module generates an extra branch from the previous lowest-resolution branch by a reduction searching block. (c) The proposed searching block that contains both convolutions with different kernel sizes C_1, C_2, C_3 and a lightweight Transformer \mathcal{T} .

values $Q, K, V \in \mathbb{R}^{n \times s^2}$. Following the standard Transformer [75], our lightweight Transformer is built upon the Multi-Head Self-Attention $\mathcal{A}(\cdot)$, which allows the model to jointly attend to information at different positions. It is defined as:

$$\begin{aligned} \mathcal{A}_{enc}(Q, K, V) &= \text{Concat}(\text{head}_1, \dots, \text{head}_h)W^O \\ \text{where } \text{head}_i &= \text{Attention}(QW_i^Q, KW_i^K, VW_i^V) \\ &= \text{softmax}\left[\frac{QW_i^Q(KW_i^K)^T}{\sqrt{d}}\right]VW_i^V \quad (3) \end{aligned}$$

where h is the number of heads, d is the hidden dimensions of the attended subspaces, and $W_i^Q, W_i^K, W_i^V \in \mathbb{R}^{s^2 \times d}$, $W^O \in \mathbb{R}^{hd \times s^2}$ are learned embeddings (weights). A position-wise Feed-Forward Network (FFN) $\mathcal{F}_{enc}(\cdot)$, which consists of two linear transformations with a ReLU activation in between, is then applied to the attended features:

$$\mathcal{F}_{enc}(x) = \max(0, xW_1 + b_1)W_2 + b_2 \quad (4)$$

where $W_1 \in \mathbb{R}^{s^2 \times 4s^2}$, $W_2 \in \mathbb{R}^{4s^2 \times s^2}$, b_1 and b_2 are the weights and biases of the linear layers respectively. We employ residual connections [35] around both the Multi-Head Self-Attention layer and the Feed-Forward Network, which are followed by layer normalization [1] as in [75].

Decoder. Our decoder follows the same paradigm of the encoder: Multi-Head Self-Attention layer and Feed-Forward Networks. It uses the output of the encoder F as keys and values and a set of n learnable s^2 -dimensional semantic embeddings $S \in \mathbb{R}^{n \times s^2}$ as queries. The decoder can be formalized as $\mathcal{F}_{dec}(\mathcal{A}_{dec}(S, F, F))$. Finally, the output of the decoder is transformed back to the proper shape by an inverse projection function $\widehat{P}(\cdot)$. Like the projector P , the inverse projector $\widehat{P}(\cdot)$ consists of a point-wise convolution (with a Batch Normalization layer) and a bilinear interpola-

tion operation. Note that since image modeling is not a sequence prediction task, and there is no temporal relationship between the semantic tokens, we remove the first Multi-Head Attention in the standard Transformer decoder [75].

Time Complexity. The time complexities of our Multi-Head Self-Attention and our FFN are $O(4nds^2 + 2n^2d)$ and $O(8ns^4)$, respectively, where s^2 , d and n are in the projected low-dimensional space. Since s^2 is a projected small spatial size, the overall time complexity (FLOPs) $O_{\mathcal{T}}(n)$ of our Transformer is approximately linear with n^2d . In the following part, we will further introduce a fine-grained search strategy to reduce the number of tokens n in order to make the lightweight Transformer more efficient.

In summary, the **main difference** between our lightweight Transformer and the standard Transformer [75, 7] lies in: (1) A projection function $P(\cdot)$ is used to learn self-attention in a low-dimensional space. (2) A simpler yet effective 2D positional map P is used for positional encoding. (3) The first Multi-Head Attention and the spatial encoding in the standard Transformer decoder are removed.

3.2. Multi-branch Search Space

Inspired by HRNet [76], we design a multi-branch search space for dense predictions that contains both multi-scale features and global contexts while maintaining high-resolution representations throughout the network.

Overview. The network consists of two modules: the parallel module and the fusion module. Both of the two modules are constructed with our searching blocks. As shown in Fig. 3 (a), after two convolutions which decrease the feature resolution to 1/4 of the input image size, we start with this high-resolution branch and gradually add high-to-low resolution branches through fusion modules, and con-

nect the multi-resolution branches in parallel through parallel modules. Finally, multi-branch features are resized and concatenated together, and connected to the final classification/regression layer without any additional heads.

The parallel module obtains larger receptive fields and multi-scale features by stacking searching blocks in each branch. It has $m \in [1, 4]$ branches containing nc_1, \dots, nc_m convolutions with nw_1, \dots, nw_m channels in each branch. A fusion module is used after a parallel module to exchange information across multiple branches. An extra lower-resolution branch is also generated from the previously lowest-resolution branch until it reaches 1/32 down-sampling ratios. A fusion module takes m_{in} branches from the previous parallel module as input and outputs m_{out} branches. For each output branch, all its neighboring input branches are fused by using the searching block to unify their feature map sizes. For example, a 1/8 output branch integrates information of 1/4, 1/8, and 1/16 input branches. In our fusion module, the high-to-low resolution feature transformation is realized by the reduction searching block, while the low-to-high resolution feature transformation is implemented with the normal searching block and upsampling.

Searching block. As shown in Fig. 3 (c), our searching block contains two paths: one path is a MixConv [73], the other path is a lightweight Transformer which aims to provide more global contexts. The number of convolutional channels and the number of tokens in the Transformer are searchable parameters.

Formally, let X be the input of c feature channels (the spatial dimension is omitted for simplicity). In the MixConv path, the first layer is a point-wise convolution \mathcal{C}_0 which expands X to a $3r \times c$ dimension (*i.e.*, the expansion ratio is $3r$); the output is split into three parts with an equal number of channels (*i.e.*, each with $r \times c$ channels), which are then fed into three depth-wise convolutions $\mathcal{C}_1, \mathcal{C}_2, \mathcal{C}_3$ with kernel sizes of $3 \times 3, 5 \times 5$, and 7×7 , respectively. The outputs of these three layers are concatenated, followed by another point-wise convolution \mathcal{C}_4 that produces the feature map with the desired number of channels c' . In the Transformer path, a lightweight Transformer \mathcal{T} with n tokens is applied to the input feature X to obtain the global self-attention. The outputs of two branches are added as the final output of the searching block. Intuitively, the Transformer path can be regarded as a residual path for enhancing the global context within the searching block. The information flow in a searching block can be written as:

$$X' = \mathcal{C}_4(\text{Concat}(\mathcal{C}_1(\mathcal{C}_0(X)_1), \mathcal{C}_2(\mathcal{C}_0(X)_2), \mathcal{C}_3(\mathcal{C}_0(X)_3))) + \mathcal{T}(X) \quad (5)$$

where $\mathcal{C}_0(X)_i$ represents the i -th part of the output of $\mathcal{C}_0(X)$, as shown in Fig. 3 (c). Note that when the strides of the convolutions $\mathcal{C}_1, \mathcal{C}_2, \mathcal{C}_3$ are equal to 2, as in the reduction searching block, the inverse projection $\widehat{\mathcal{P}}(\cdot)$ in Transformer

resizes its input into half size of the original spatial dimension in order to match the output shape of \mathcal{C}_4 .

3.3. Resource-aware Fine-grained Search

Our supernet is a multi-branch network where each branch is a chain of searching blocks operating at different resolutions; each searching block combines a MixConv and a Transformer. Unlike previous searching methods that are designed for specific tasks, we aim to customize the network for various tasks. Specifically, we propose a resource-aware channel/query-wise fine-grained search strategy to explore the optimal feature combination for different tasks.

We adopt a progressive shrinking NAS paradigm which generates lightweight models by discarding some of the convolutional channels and Transformer queries during training. As described in [56], as channels in depth-wise convolutions are independent in our searching block, any channels from these convolutions can be easily removed without affecting the other searching blocks; we only need to remove the corresponding weights from the convolutions. Similarly, if a token of the Transformer is discarded, we just remove the corresponding weights from the 1×1 convolutions of the projections $\mathcal{P}(\cdot)$ and $\widehat{\mathcal{P}}(\cdot)$, and the corresponding embedding from queries S .

In the rest of this paper, we call a channel of the depth-wise convolutions or a token in Transformers a *search unit*. A searching block with c input channels, the expansion ratio of $3r$, and n tokens has $3rc + n$ search units in total.

Following Darts [50], we introduce an importance factor $\alpha > 0$ that can be learned jointly with the network weights for each search unit of the searching block. We then progressively discard those with low importance while maintaining overall performance. Inspired by works on channel pruning [89, 52, 56], we add a resource-aware L1 penalty on α , which effectively pushes importance factors of high computational costs to zero. Specifically, the L1 penalty of a search unit is weighted by the amount of the reduction in computational cost $\Delta > 0$ (*i.e.* FLOPs in this case):

$$\Delta_i = \begin{cases} 3 \times 3 \times h \times w, & i \in [0, rc] \\ 5 \times 5 \times h \times w, & i \in [rc, 2rc] \\ 7 \times 7 \times h \times w, & i \in [2rc, 3rc] \\ O_{\mathcal{T}}(n') - O_{\mathcal{T}}(n' - 1), & i \in [3rc, 3rc + n] \end{cases} \quad (6)$$

where $O_{\mathcal{T}}$ is the FLOPs of the Transformer defined in Sec. 3.1, i is the index of the search unit, n' is the number of remaining tokens. Note that Δ 's for search units of convolutions are fixed, while in the Transformer, Δ 's is a function of the number of remaining tokens. It is worth mentioning that, although FLOPs is not always a good measure of latency, we use it anyway as it is the most widely and easily used metric. The Eq. 7 can be easily adapted to use other metrics, *e.g.*, latency and energy cost.

With the added resource-aware penalty term, the overall training loss is:

$$L = L_{\text{task}} + \lambda \sum_{i \in [0, 3rc+n)} \Delta_i |\alpha_i| \quad (7)$$

where L_{task} denotes the standard classification/regression loss, and λ denotes the coefficient of the L1 penalty term.

During training, after every few epochs, we progressively remove the search units whose importance factors are below a predefined threshold ϵ and re-calibrate the running statistics of Batch Normalization (BN) layers. Note that if all tokens of a Transformer are removed, the Transformer will degenerate into a residual path, as shown in Fig. 2.

When the search ends, the remaining structure not only represents the best accuracy-efficiency trade-offs, but also has the optimal low-level/high-level and local/global feature combination for a specific task. In addition, since the network training and architecture search are conducted in a unified end-to-end manner, the resulting network can be used directly without fine-tuning.

4. Experiments

4.1. Implementation Details

To validate the generalizability of our method, we select five benchmark datasets on four representative tasks for performance evaluation: image classification on ImageNet [21], human pose estimation on COCO keypoint [48], semantic segmentation on Cityscapes [17] and ADE20K [95], and 3D object detection on KITTI [30]. These benchmarks are carefully selected as they require different receptive fields, global/local contexts, and 2D/3D perceptions. In this work, the same supernet is used for all five benchmarks; It begins with two 3×3 convolutions with stride 2, which is followed by five parallel modules (respectively with 1, 2, 3, 4, 4 branches); a fusion module is inserted between every two adjacent parallel modules, to obtain multi-scale features. For Transformers, we set $s = 8$, $d = s^2 = 64$, and $h = 1$. In some evaluation experiments without search, we fix $d = 8$. The expansion ratio r of the searching block is set to be 4. For the MixConv, we use the scales from the batch normalization layers after the depth-wise convolutions as the importance factors; for the Transformer, we use the scales from the batch normalization layer in the projector \mathcal{P} as the importance factors. On each benchmark, we obtain HR-NAS-A and HR-NAS-B using different λ values. Search units with $\alpha < 0.001$ are deemed unimportant and removed every five epochs. Unless specified, all experiments in this paper use standard training protocols, *e.g.*, we don't apply techniques like AutoAug [18], Mixup [90], and Cutout [23]. All our models are trained from scratch without pretraining on the ImageNet dataset, and are evaluated with single-scale input and without multicrop. Details of the datasets and the training settings for each task can be found in Supplemental Materials.

Table 1. Comparision with state-of-the-arts on ImageNet under the mobile setting. \dagger denotes methods using Swish activation [62], \ddagger denotes methods trained on AutoAugment [18] or RandAugment [19]. FLOPs is measured using an input size of 224×224 .

Model	Params	FLOPs	Top-1(%)
CondenseNet [39]	2.9M	274M	71.0
ShuffleNetV1 [93]	3.4M	292M	71.5
ShuffleNetV2 [55]	3.5M	299M	72.6
MobileNetV2 [65]	3.4M	300M	72.0
MobileNetV3 [36] \dagger	5.4M	219M	75.2
EfficientNet-B0 [72] $\dagger\dagger$	5.3M	390M	77.3
FBNet-B [79]	4.5M	295M	74.1
AutoSlim-MobileNetV2 [87]	5.7M	305M	74.2
Proxyless [6]	4.1M	320M	74.6
DA-NAS [20]	—	323M	74.3
AtomNAS-A [56]	3.9M	258M	74.6
SinglePathOneShot [34]	3.4M	328M	74.7
FairNAS-C [16]	4.4M	321M	74.7
MnasNet-A1 [71]	3.9M	312M	75.2
TF-NAS-C [38]	—	284M	75.2
SCARLET-B [15]	6.5M	329M	76.3
ST-NAS-A [33]	5.2M	326M	76.4
HR-NAS-A	5.5M	267M	75.7
HR-NAS-B	6.4M	325M	76.5
MixNet-S [73] \dagger	4.1M	256M	75.8
AtomNAS-A+ [56] \dagger	4.7M	260M	76.3
Once-for-all [5] \dagger	4.4M	230M	76.0
Once-for-all (finetuned) [5] \dagger	4.4M	230M	76.9
BigNAS [88] $\dagger\dagger$	4.5M	242M	76.5
FairNAS-C+ [16] \dagger	5.6M	325M	76.7
HR-NAS-A \ddagger	5.5M	267M	76.6
HR-NAS-B \ddagger	6.4M	325M	77.3

4.2. Comparative Results

We conduct experiments against the state-of-the-art methods on five benchmarks: image classification on ImageNet (Tab. 1), semantic segmentation on Cityscapes (Tab. 2), semantic segmentation on ADE20K (Tab. 3), human pose estimation on COCO keypoint (Tab. 4), and 3d object detection on KITTI (Tab. 5). From these tables we can see that: (1) Our method achieves state-of-the-art performance on all three dense prediction tasks and competitive results on the classification task. Compared with other tasks, classification usually benefits less from multi-scale and global contexts because it aggregates position-invariant features through global pooling. (2) Many existing methods, such as [88, 47, 44] utilize additional modules or pre-training on the ImageNet dataset to get better performance for a specific task. In contrast, our method is able to show superior results across multiple challenging datasets without any bells and whistles. (3) We evaluate the mean and standard deviation of 5 runs on Cityscapes [17] with Random Search [45] as a baseline. It shows that our method yields stable results with a standard deviation of about only 0.3. (4) For NAS methods toward high segmentation accuracy [49, 28] rather than accuracy-efficiency trade-offs,

Table 2. Comparative results on the CityScapes validation set (mIoU,%). * indicates the model is pre-trained on the ImageNet dataset. FLOPs is measured using an input size of 512×1024 . † denotes the model is reduced by us for acc-efficiency trade-offs.

Model	Params	FLOPs	mIoU(%)
SegNet [2]	29.47M	649G	57.00
Enet [60]	0.37M	8.69G	58.30
BiSeNet [86]	5.8M	6.58G	69.00
MobileNetV2 [65]	2.11M	5.33G	70.71
MobileNetV3-Large [36]	1.51M	2.48G	72.36
HRNet-W18-Small [76]	3.94M	19.30G	75.44
C3 [59]	0.20M	6.45G	61.96
SkipNet-MobileNet [68]*	—	13.80G	62.40
EDANet [53]	0.68M	7.98G	65.11
SwiftNet [58]	11.80M	26G	70.20
DFANet [44]*	7.8M	1.7G	70.30
ShuffleNetV2+DPC [74]	3.00M	6.92G	71.30
Auto-DeepLab [49]-Tiny†	3.16M	27.29G	71.21
GAS [47]*	1.50M	—	71.80
SqueezeNAS-Large [66]	0.73M	8.35G	72.40
SpineNet-49 [28]-Tiny†	5.49M	37.99G	74.18
Random Search [45]	6.11 ± 2.25 M	7.09 ± 1.88 G	70.20 ± 3.01
HR-NAS-A	2.20 ± 0.14 M	1.91 ± 0.11 G	74.26 ± 0.37
HR-NAS-B	3.85 ± 0.19 M	4.66 ± 0.17 G	75.90 ± 0.30

Table 3. Comparative results on the ADE20K validation set (mIoU,%). FLOPs is measured using an input size of 512×512 .

Model	Params	FLOPs	mIoU(%)
MobileNetV2[65]	2.20M	2.76G	32.04
MobileNetV3-Large[36]	1.60M	1.32G	32.31
HRNet-W18-Small [76]	3.97M	10.23G	33.41
HR-NAS-A	2.49M	1.42G	33.22
HR-NAS-B	3.86M	2.19G	34.92

we reduce their network width to 1/2 (and depth to 1/2 for [49]), thus obtain the tiny variants. Our method outperforms the second-best competitor by a large margin on Cityscapes (74.18 vs. 76.01), ADE20K (33.41 vs. 34.92), and COCO keypoint (74.9 vs. 75.5) using a much lighter model, showing its superiority and accuracy-efficiency balance ability on dense prediction tasks.

4.3. Ablation Study

Search Space. In this part, we study the design components of our search space. In Tab. 6 we show how the introduction of different components affects the performance and FLOPs, using the Cityscapes segmentation benchmark as an example. The baseline search space, “Single-branch” in Tab. 6, is a single-branch network with only 3×3 convolutions, where the up-sampling operations are applied at the end for dense prediction tasks. Adding the multi-branch architecture increases the mIoU from 66.23% to 68.65% with fewer parameters and FLOPs, showing the effectiveness of our multi-branch design. The MixConv with a mix of 3×3 , 5×5 , 7×7 convolutions in the searching block further improves the mIoU by 3.34%. Finally, the lightweight Transformer provides another gain of 2.56% (71.99% v.s. 74.55%) with only extra 70M FLOPs.

Table 4. Comparisons on COCO keypoint validation set. * indicates the model is pre-trained on the ImageNet dataset. Params and FLOPs are calculated for the pose estimation network, and those for human detection and keypoint grouping are not included.

Method	Input size	Params	FLOPs	AP	AP ^M	AP ^L	AR
ShuffleNetV1 [93]*	256×192	1.0M	0.16G	58.5	55.2	64.6	65.1
ShuffleNetV2 [55]*	256×192	1.3M	0.17G	59.8	56.5	66.2	66.4
MobileNetV2 [65]*	256×192	2.3M	0.33G	64.6	61.0	71.1	70.7
NAS-CSS [57]	256×192	2.9M	1.48G	65.9	63.1	70.0	69.3
DA-NAS [20]	256×192	10.9M	2.18G	68.4	65.5	74.4	75.7
CPN [12]	256×192	27.0M	6.20G	69.4	—	—	—
SimpleBaseline-50 [81]*	256×192	34.0M	8.90G	70.4	67.1	77.2	76.3
HRNet-W32 [76]	256×192	28.5M	7.10G	73.4	70.2	80.1	78.9
AutoPose [32]	256×192	—	10.65G	73.6	69.8	79.7	78.1
HR-NAS-A	256×192	1.7M	0.25G	67.7	65.4	71.1	70.8
HR-NAS-B	256×192	6.1M	1.35G	73.7	70.2	80.6	79.3
ShuffleNetV1 [93]*	384×288	1.0M	0.35G	62.2	57.8	69.5	68.4
ShuffleNetV2 [55]*	384×288	1.3M	0.37G	63.6	59.5	70.7	69.7
MobileNetV2 [65]*	384×288	2.3M	0.74G	67.3	62.8	74.7	72.8
SimpleBaseline-50 [81]*	384×288	34.0M	20.02G	72.2	68.1	79.7	77.6
PoseNFS-3 [84]	384×288	15.8M	14.8G	73.0	—	—	—
HRNet-W32 [76]	384×288	28.5M	16.0G	74.9	71.5	80.8	79.3
HR-NAS-A	384×288	1.1M	0.35G	65.7	62.5	72.1	71.4
HR-NAS-B	384×288	6.6M	3.72G	75.5	72.6	81.7	79.4

Table 5. Vehicle 3D detection results(AP,%) on the KITTI split validation set. All methods are implemented based on the Pointpillar [43] framework. FLOPs is calculated for 2D RPN network using an input size of 496×432 .

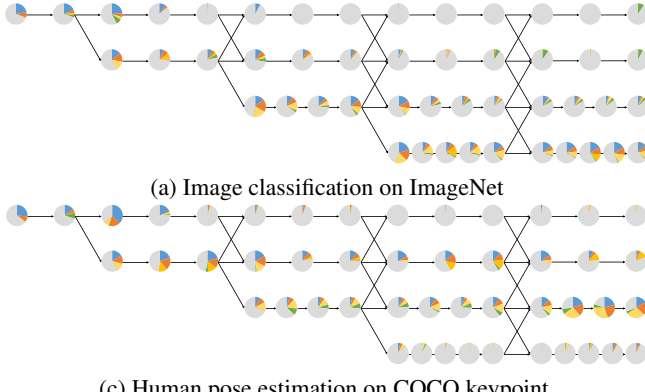
Method	Params	FLOPs	Moderate	Easy	Hard
ShuffleNetV2 [55]	1.69M	2.26G	66.73	80.74	61.84
MobileNetV2 [65]	2.49M	6.47G	67.65	82.52	64.22
Pointpillar [43]	4.80M	61.75G	77.12	86.61	72.71
HR-NAS-A	2.13M	3.22G	69.74	83.09	64.89
HR-NAS-B	4.74M	15.65G	78.49	87.62	75.53

Table 6. Ablation study of our search space on the CityScapes semantic segmentation validation set.

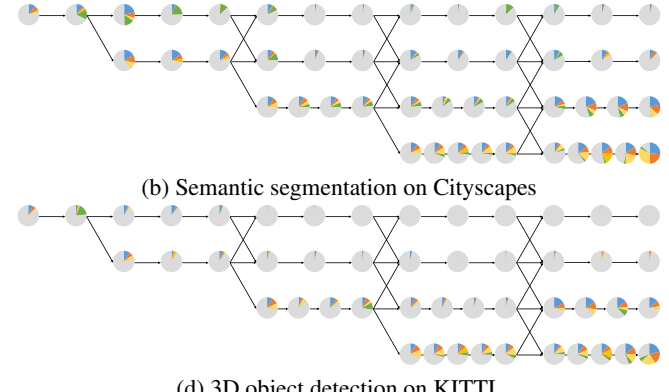
Method	Params	FLOPs	mIoU(%)	mACC(%)	aACC(%)
Single-branch	1.59M	1.81G	66.23	75.57	94.43
Multi-branch	0.82M	1.64G	68.65	78.26	94.80
+MixConv	1.12M	1.86G	71.99	80.33	95.40
+Transformer	2.23M	1.93G	74.55	82.98	95.54

Lightweight Transformer. In Tab. 7, we study the choice of positional embeddings. It can be seen that using the proposed 2D positional map in the encoder of the Transformer achieves better performance than using the sinusoidal position encoding [75] and the learned position embedding [22]. This may be because our lightweight Transformer has fewer queries and smaller token dimensions than the other two, and therefore it is unnecessary to use high dimension representation for position information. We also evaluate the alternative which uses the 2D positional map at both the encoder and the decoder; the performance is slightly worse than the encoder-only option.

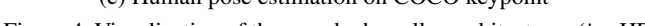
The proposed Transformer can be used as a plug-and-play component. To show this, we add our Transformer to the Inverted Residual Blocks of two efficient models ShuffleNetV2 [55] and MobileNetV2 [65], and eval-



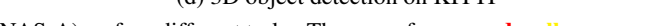
(a) Image classification on ImageNet



(b) Semantic segmentation on Cityscapes



(c) Human pose estimation on COCO keypoint



(d) 3D object detection on KITTI

Figure 4. Visualization of the searched smaller architectures (*i.e.* HR-NAS-A) on four different tasks. The area of **cyan**, **red**, **yellow**, **green**, and **gray** sectors indicate the number of 3×3 , 5×5 , 7×7 convolutional channels, the number of transformer queries, and the number of removed channels/queries, respectively. Note that if all queries and convolutional channels of a searching block are removed, the searching block will degenerate into a residual path. For simplicity, we only visualize searching blocks in the parallel module. We can see that our method is able to find different architectures for different tasks, showing that it can automatically adapt to various tasks.

Table 7. Comparisons (%) of different positional embedding of Transformer with $n = 8$ and $s = 8$ on Cityscapes validation set. ‘Enc’ and ‘Dec’ denote the positional embedding are employed in the encoder and decoder of the Transformer, respectively. FLOPs is measured using an input size of 512×1024 .

Input size	Params	FLOPs	mIoU	mACC	aACC
Baseline	1.120M	1.863G	71.99	80.33	95.40
Sinusoidal position encoding	2.346M	2.131G	71.91	80.38	95.08
Learned position embedding	2.930M	2.236G	72.71	80.88	95.33
2D positional map (Enc only)	2.273M	1.872G	74.22	82.36	95.52
2D positional map (Enc + Dec)	2.278M	1.873G	73.70	81.89	95.47

ate their performance on both ImageNet classification and Cityscapes segmentation tasks. PSP module [94] is added as segmentation head to all models. As shown in Tab. 8, our Transformer improves the two baseline models on both classification and segmentation tasks.

4.4. Visualization of Searched Networks

We visualized the four smaller models we found on each of the four benchmarks (*i.e.* HR-NAS-A) in Fig. 4. We can observe that our method can find different architectures for different tasks, showing that it can automatically adapt to various tasks: (1) In the image classification task and the 3D detection task, at the high-resolution branches (*i.e.* first and second branches), the models we found remove most of the search units; some searching blocks are even completely removed, as indicated by circles with complete gray in Fig. 4). The reason is that in these two tasks, global semantic information is more important than local information. (2) The model for the segmentation task still retains computation from the first two branches, as it is important to keep high resolution imagery for semantic segmentation tasks. (3) The human pose estimation model mainly utilizes the second and the third branches, which means it may

Table 8. Single-crop top-1 error rates (%) on the ImageNet, and the mIoU (%) on the cityscapes dataset. All models are trained from scratch. FLOPs is measured using classification models.

Method	Params	FLOPs	top-1	mIoU
ShuffleNetV2 [55]	2.279M	0.150G	69.5	66.02
ShuffleNetV2 [55] + transformer	2.758M	0.157G	70.1	67.31
MobileNetV2 [65]	3.505M	0.319G	72.0	68.98
MobileNetV2 [65] + transformer	3.770M	0.321G	72.8	70.17

rely more on middle-resolution semantics instead of high-resolution semantics. (4) Transformers are more used in the segmentation and the human keypoint estimation tasks, indicating these dense prediction tasks benefit more from global contexts.

5. Conclusion

In this paper, we introduce a lightweight and plug-and-play Transformer that can be easily combined with convolutional networks to enrich global contexts for dense image prediction tasks. We then effectively encode both the proposed Transformers and convolutions into a well-designed high-resolution search space to model both global and multiscale contextual information. A channel/query-level fine-grained progressive shrinking strategy is applied to the search space for searching and customizing efficient models for various tasks. Our searched models achieve state-of-the-art trade-offs between performance and FLOPs for three dense prediction tasks and an image classification task, given only small computational budgets.

Acknowledgements Ping Luo was supported by the General Research Fund of HK No.27208720. Zhiwu Lu was supported by National Natural Science Foundation of China (61976220 and 61832017), and Beijing Outstanding Young Scientist Program (BJJWZYJH012019100020098).

A. Datasets and Settings

In this section, we provide details of the datasets and settings used. We use the same super network for training and evaluation in each task.

In practice, different hyperparameters are often tuned with a validation set for different tasks according to different datasets and losses. For example, HRNet [76] is trained using two different settings for segmentation and keypoint estimation tasks. In this work, we follow the common training settings [24] of each task, *i.e.*, the setting in HRNet [76] for segmentation and keypoint estimation, AtomNAS [56] for classification, and PointPillar [43] for 3D detection.

As for the choice of λ for each task, we first empirically tuned it so that HR-NAS-A’s FLOPs is comparable to the least FLOPs among the baseline models, then we relaxed the restriction so that HR-NAS-B reaches SOTA yet still costs less FLOPs than the best baseline models. Currently, the searched model size cannot be controlled precisely by λ . We will strengthen it by incorporating other techniques as our future work. See below for details.

ImageNet for Image Classification. The ILSVRC 2012 classification dataset [21] consists of 1,000 classes, with a number of 1.2 million training images and 50,000 validation images. Follow the common practice in [71, 85, 56, 72, 70], we adopt a RMSProp optimizer with momentum 0.9 and weight decay 1e-5; exponential moving average (EMA) with decay 0.9999; and exponential learning rate decay. The input size is 224×224 . The initial learning rate is set to 0.064 with batch size 1024 on 16 Tesla V100 GPUs for 350 epochs, and decays by 0.97 every 2.4 epochs. By setting the coefficient of the L1 penalty term λ to 1.8e-4 and 1.2e-4, we obtain our HR-NAS-A and HR-NAS-B. Unless specified, we adopt the ReLU activation and the basic data augmentation scheme, *i.e.*, random resizing and cropping, and random horizontal flipping, and use single-crop for evaluation. For experiments of HR-NAS $\dagger\dagger$, we also adopt the SE module [37], Swish activation [62], and RandAugment [19] for better performance. We report the top-1 Accuracy as the evaluation metric.

Cityscapes for Semantic Segmentation. The Cityscapes dataset [17] contains high-quality pixel-level annotations of 5000 images with size 1024×2048 (2975, 500, and 1525 for the training, validation, and test sets respectively) and about 20000 coarsely annotated training images. Following works [26, 17], 19 semantic labels are used for evaluation without considering the void label. In this work, the input size is set to 512×1024 . We use an AdamW optimizer with momentum 0.9 and weight decay 1e-5; exponential moving average (EMA) with decay 0.9999. The initial learning rate is set to 0.04 with batch size 32 on 8 Tesla V100 GPUs for 430 epochs. The learning rate and momentum follow the onecycle scheduler with a minimum learning rate of 0.0016. By setting the coefficient of the L1 penalty

term λ to 1.6e-4 and 6.0e-5, we obtain our HR-NAS-A and HR-NAS-B. We use a basic data augmentation, *i.e.*, random resizing and cropping, random horizontal flipping, and photometric distortion for training and single-crop testing with a test size of 1024×2048 . We report the mean Intersection over Union (mIoU), mean (macro-averaged) Accuracy (mAcc), and overall (micro-averaged) Accuracy (aAcc) as the evaluation metrics.

ADE20K for Semantic Segmentation. The ADE20K dataset [95] contains 150 classes and diverse scenes with 1,038 image-level labels. The dataset is divided into 20K/2K/3K images for training, validation, and testing respectively. In this work, the input size and testing size is set to 512×512 and 512×2048 , respectively. The model is trained with a batch size of 64 on 8 Tesla V100 GPUs for 200 epochs. We use the same optimizer, learning rate scheduler, data augmentation, and penalty weight λ as in the Cityscapes dataset. We report the mean Intersection over Union (mIoU) as the evaluation metric.

COCO Keypoint for Human Pose Estimation. The COCO dataset [48] contains over 200,000 images and 250,000 person instances labeled with 17 keypoints. We train our model on the COCO train2017 set, including 57K images and 150K person instances. We evaluate our approach on the val2017, containing 5000 images. In this work, we train the model using input sizes of 256×192 and 384×288 with batch size 384 and 192 on 8 Tesla V100 GPUs for 210 epochs, respectively. Following HRNet [76], the initial learning rate is set to 1e-3 with a multistep scheduler (decayed by a factor of 0.1 in 170 and 200 epochs). We use an Adam optimizer with momentum 0.9 and weight decay 1e-8; exponential moving average (EMA) with decay 0.9999. By setting the coefficient of the L1 penalty term λ to 1e-6 and 1e-8, we obtain our HR-NAS-A and HR-NAS-B. We use random scaling and rotation as only data augmentation for training and single-crop testing. We report average precision (AP), recall scores (AR), AP^M for medium objects, and AP^L for large objects as evaluation metrics.

KITTI for 3D Object Detection. The KITTI 3D object detection dataset [30] is widely used for monocular and LiDAR-based 3D detection. It consists of 7,481 training images and 7,518 test images as well as the corresponding point clouds and the calibration parameters, comprising a total of 80,256 2D-3D labeled objects with three object classes: Car, Pedestrian, and Cyclist. Each 3D ground truth box is assigned to one out of three difficulty classes (easy, moderate, hard) according to the occlusion and truncation levels of objects. In this work, we follow the train-val split [11], which contains 3,712 training and 3,769 validation images. The overall framework is based on Pointpillars [43]. The input point points are projected into bird’s-eye view (BEV) feature maps by a voxel feature encoder (VFE). The projected BEV feature maps (496×432) are then used as

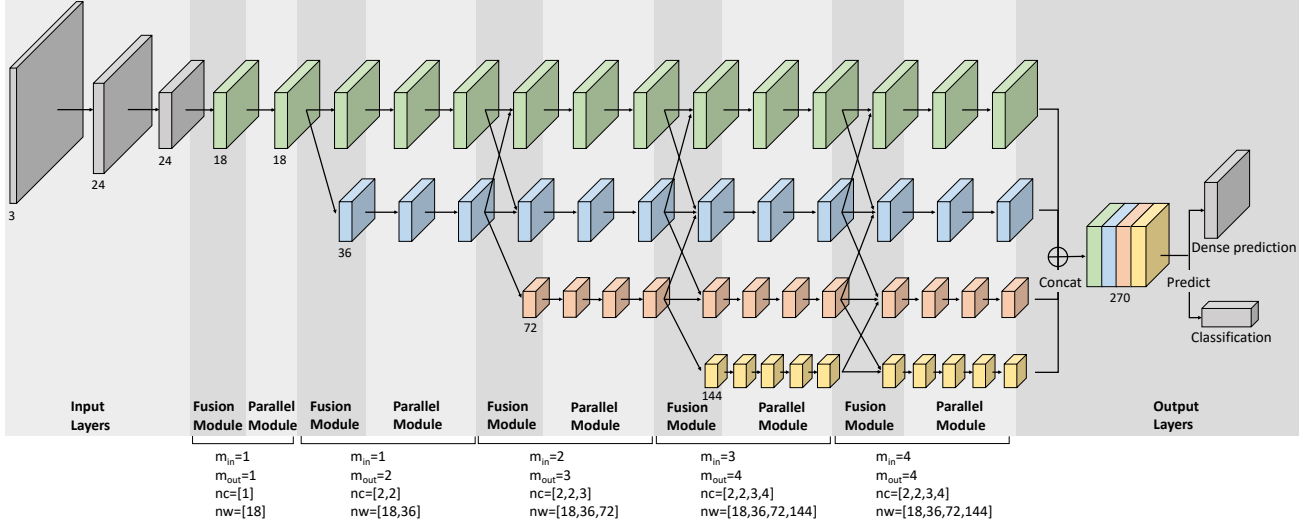


Figure 5. Visualization of our super network architecture. m_{in} and m_{out} denote the input and output numbers of branches in the fusion module. nc and nw denote the number of searching blocks and the number of channels in the parallel module, respectively. The arrows represent the searching blocks and the cubes represent the feature maps. The number under the cube represents the number of channels.

input of our 2D network for 3D/BEV detection. Following [43, 25], we set, pillar resolution: 0.16m, max number of pillars: 12000, and max number of points per pillar: 100. We use the onecycle scheduler with an initial learning rate of 2e-3, a minimum learning rate of 2e-4, and batch size 16 on 8 Tesla V100 GPUs for 80 epochs. We use an AdamW optimizer with momentum 0.9 and weight decay 1e-2. We apply the same data augmentation, *i.e.*, random mirroring and flipping, global rotation and scaling, and global translation for 3D point clouds as in Pointpillar [43]. At inference time, we apply axis-aligned nonmaximum suppression (NMS) with an overlap threshold of 0.5 IoU. We report standard average precision (AP) as the evaluation metric.

B. Network Architecture

As shown in Fig. 5, we visualize our entire super network used in all experiments. It begins with two 3×3 convolutions with stride 2 and number of channels 24, which are followed by five parallel modules (respectively with 1, 2, 3, 4, 4 branches); a fusion module is inserted between every two adjacent parallel modules, to obtain multi-scale features. The numbers of channels for the four branches in parallel modules are 18, 36, 72, 144, respectively.

C. Ablative Results for Transformer

In this section, we conduct two ablative experiments to study the impact of the projection size s , the encoder-decoder structure, and the attention mechanism on the performance of our lightweight Transformer. For both experiments, we take the searched network on Multi-branch + MixConv space (without Transformer) in Tab.6 of the main paper as a strong baseline.

Table 9. Comparisons of different projection size s of Transformer on the CityScapes validation set. The query number n is set to 8.

Input size	Params	FLOPs	mIoU(%)	mACC(%)	aACC(%)
Baseline	1.120M	1.863G	71.99	80.33	95.40
2×2	1.180M	1.863G	72.27	80.74	95.40
4×4	1.246M	1.864G	73.32	81.76	95.45
8×8	2.273M	1.872G	74.22	82.36	95.52
16×16	18.543M	1.969G	74.18	82.07	95.50

Table 10. Ablation study of our lightweight Transformer with $n = 8$ and $s = 8$ on the CityScapes validation set. Notations: ‘Enc’ – only the encoder of Transformer is used, ‘Enc + Dec’ – both the encoder and decoder are used in Transformer, ‘channel’ – use each channel as a token, ‘spatial’ – use each spatial position as a token.

Input size	Params	FLOPs	mIoU(%)	mACC(%)	aACC(%)
Baseline	1.120M	1.863G	71.99	80.33	95.40
SE [37]	2.101M	1.864G	72.81	81.33	95.35
Non-local [78]	1.317M	2.951G	72.50	81.32	95.34
Enc (spatial)	1.184M	1.866G	72.61	80.97	95.26
Enc (channel)	1.723M	1.869G	73.66	82.10	95.50
Enc + Dec (spatial)	1.204M	1.867G	73.54	81.87	95.44
Enc + Dec (channel)	2.273M	1.872G	74.22	82.36	95.52

Projection Sizes. We evaluate our Transformers with different projected spatial sizes s . From Tab. 9 we can see that when s goes from 0 to 8, the mIoU keeps increasing at the expense of small extra cost (*i.e.*, FLOPs). Further increasing s brings no gain in performance but drastically increasing FLOPs. We therefore choose $s = 8$ throughout the experiments.

Attention Structures and Mechanisms. We also conduct ablative experiments to validate the effectiveness of our Transformer. We discuss (1) encoder-decoder structures and (2) two kinds of attention mechanisms by transposing the feature, *i.e.*, ‘channel’ – use each channel of the flattened feature map as a token, ‘spatial’ – use each spatial po-

sition as a token. As shown in Tab. 10, our Transformer obtains the best performance when both encoder and decoder are used on channel-wise tokens. Our Transformer also significantly outperforms its counterparts such as SE [37] and Non-local [78] on dense prediction tasks. Since the channel-wise lightweight transformer shows better performance, we set it as the default in this work.

D. Visualization of Visual Recognition Results

We visualize the results of HR-NAS-A on segmentation, human pose estimation, and 3D detection (Fig. 6, 7, 8).

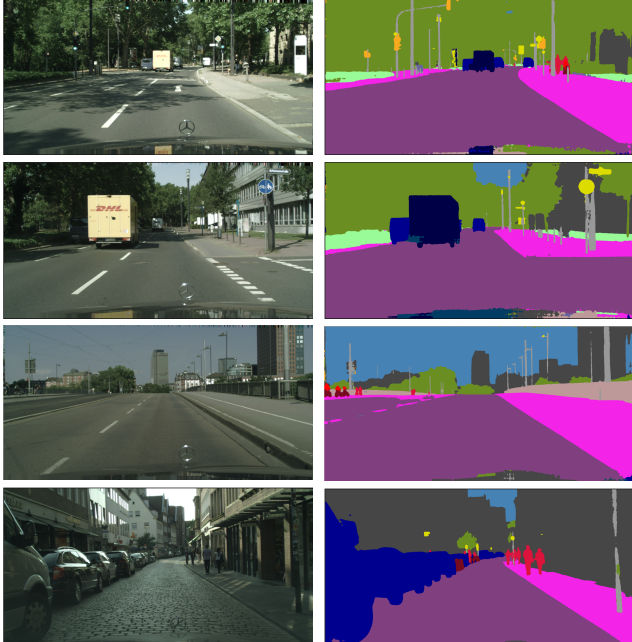


Figure 6. Visualization of semantic segmentation results (left: original images; right: segmentation maps) on Cityscapes.

References

- [1] Jimmy Lei Ba, Jamie Ryan Kiros, and Geoffrey E Hinton. Layer normalization. *arXiv preprint arXiv:1607.06450*, 2016. 4
- [2] Vijay Badrinarayanan, Alex Kendall, and Roberto Cipolla. Segnet: A deep convolutional encoder-decoder architecture for image segmentation. *IEEE TPAMI*, 39(12):2481–2495, 2017. 7
- [3] Gabriel Bender, Pieter-Jan Kindermans, Barret Zoph, Vijay Vasudevan, and Quoc Le. Understanding and simplifying one-shot architecture search. In *ICML*, pages 550–559, 2018. 3
- [4] Tom B Brown, Benjamin Mann, Nick Ryder, Melanie Subbiah, Jared Kaplan, Prafulla Dhariwal, Arvind Neelakantan, Pranav Shyam, Girish Sastry, Amanda Askell, et al. Language models are few-shot learners. *arXiv preprint arXiv:2005.14165*, 2020. 2



Figure 7. Visualization of human pose estimation on COCO.



Figure 8. Visualization of 3D object detection results on KITTI.

- [5] Han Cai, Chuang Gan, Tianzhe Wang, Zhekai Zhang, and Song Han. Once-for-all: Train one network and specialize it for efficient deployment. In *ICLR*, 2020. 1, 3, 6
- [6] Han Cai, Ligeng Zhu, and Song Han. Proxylessnas: Direct neural architecture search on target task and hardware. In *ICLR*, 2019. 1, 3, 6
- [7] Nicolas Carion, Francisco Massa, Gabriel Synnaeve, Nicolas Usunier, Alexander Kirillov, and Sergey Zagoruyko. End-to-end object detection with transformers. In *ECCV*, 2020. 2, 3, 4
- [8] Liang-Chieh Chen, Maxwell Collins, Yukun Zhu, George Papandreou, Barret Zoph, Florian Schroff, Hartwig Adam, and Jon Shlens. Searching for efficient multi-scale architectures for dense image prediction. In *NeurIPS*, pages 8699–8710, 2018. 1, 3
- [9] Liang-Chieh Chen, George Papandreou, Iasonas Kokkinos, Kevin Murphy, and Alan L Yuille. Deeplab: Semantic image segmentation with deep convolutional nets, atrous convolution, and fully connected crfs. *IEEE TPAMI*, 40(4):834–848, 2017. 2
- [10] Mark Chen, Alec Radford, Rewon Child, Jeff Wu, Hee woo Jun, Prafulla Dhariwal, David Luan, and Ilya Sutskever.

- Generative pretraining from pixels. In *ICML*, 2020. 2
- [11] Xiaozhi Chen, Kaustav Kundu, Yukun Zhu, Andrew G Berneshawi, Huimin Ma, Sanja Fidler, and Raquel Urtasun. 3d object proposals for accurate object class detection. In *NeurIPS*, pages 424–432, 2015. 9
- [12] Yilun Chen, Zhicheng Wang, Yuxiang Peng, Zhiqiang Zhang, Gang Yu, and Jian Sun. Cascaded pyramid network for multi-person pose estimation. In *CVPR*, pages 7103–7112, 2018. 7
- [13] Yukang Chen, Tong Yang, Xiangyu Zhang, Gaofeng Meng, Chunhong Pan, and Jian Sun. Detnas: Neural architecture search on object detection. *arXiv preprint arXiv:1903.10979*, 1(2):4–1, 2019. 3
- [14] Rewon Child, Scott Gray, Alec Radford, and Ilya Sutskever. Generating long sequences with sparse transformers. *arXiv preprint arXiv:1904.10509*, 2019. 2
- [15] Xiangxiang Chu, Bo Zhang, Jixiang Li, Qingyuan Li, and Ruijun Xu. Scarletnas: Bridging the gap between scalability and fairness in neural architecture search. *arXiv preprint arXiv:1908.06022*, 2019. 6
- [16] Xiangxiang Chu, Bo Zhang, Ruijun Xu, and Jixiang Li. Fairnas: Rethinking evaluation fairness of weight sharing neural architecture search. *arXiv preprint arXiv:1907.01845*, 2019. 6
- [17] Marius Cordts, Mohamed Omran, Sebastian Ramos, Timo Rehfeld, Markus Enzweiler, Rodrigo Benenson, Uwe Franke, Stefan Roth, and Bernt Schiele. The cityscapes dataset for semantic urban scene understanding. In *CVPR*, pages 3213–3223, 2016. 6, 9
- [18] Ekin D Cubuk, Barret Zoph, Dandelion Mane, Vijay Vasudevan, and Quoc V Le. Autoaugment: Learning augmentation policies from data. *arXiv preprint arXiv:1805.09501*, 2018. 6
- [19] Ekin D Cubuk, Barret Zoph, Jonathon Shlens, and Quoc V Le. Randaugment: Practical automated data augmentation with a reduced search space. In *CVPRW*, pages 702–703, 2020. 6, 9
- [20] Xiyang Dai, Dongdong Chen, Mengchen Liu, Yinpeng Chen, and Lu Yuan. Da-nas: Data adapted pruning for efficient neural architecture search. *arXiv preprint arXiv:2003.12563*, 2020. 1, 3, 6, 7
- [21] Jia Deng, Wei Dong, Richard Socher, Li-Jia Li, Kai Li, and Li Fei-Fei. Imagenet: A large-scale hierarchical image database. In *CVPR*, pages 248–255. Ieee, 2009. 6, 9
- [22] Jacob Devlin, Ming-Wei Chang, Kenton Lee, and Kristina Toutanova. Bert: Pre-training of deep bidirectional transformers for language understanding. *arXiv preprint arXiv:1810.04805*, 2018. 2, 7
- [23] Terrance DeVries and Graham W Taylor. Improved regularization of convolutional neural networks with cutout. *arXiv preprint arXiv:1708.04552*, 2017. 6
- [24] Mingyu Ding, Yuqi Huo, Haoyu Lu, Linjie Yang, Zhe Wang, Zhiwu Lu, Jingdong Wang, and Ping Luo. Learning versatile neural architectures by propagating network codes. *arXiv preprint arXiv:2103.13253*, 2021. 1, 2, 9
- [25] Mingyu Ding, Yuqi Huo, Hongwei Yi, Zhe Wang, Jianping Shi, Zhiwu Lu, and Ping Luo. Learning depth-guided convolutions for monocular 3d object detection. In *CVPR*, 2021. 10
- [26] Mingyu Ding, Zhe Wang, Bolei Zhou, Jianping Shi, Zhiwu Lu, and Ping Luo. Every frame counts: joint learning of video segmentation and optical flow. In *AAAI*, volume 34, pages 10713–10720, 2020. 9
- [27] Alexey Dosovitskiy, Lucas Beyer, Alexander Kolesnikov, Dirk Weissenborn, Xiaohua Zhai, Thomas Unterthiner, Mostafa Dehghani, Matthias Minderer, Georg Heigold, Sylvain Gelly, et al. An image is worth 16x16 words: Transformers for image recognition at scale. *arXiv preprint arXiv:2010.11929*, 2020. 2
- [28] Xianzhi Du, Tsung-Yi Lin, Pengchong Jin, Golnaz Ghiasi, Mingxing Tan, Yin Cui, Quoc V Le, and Xiaodan Song. Spinenet: Learning scale-permuted backbone for recognition and localization. In *CVPR*, pages 11592–11601, 2020. 3, 6, 7
- [29] Jiemin Fang, Yuzhu Sun, Qian Zhang, Yuan Li, Wenyu Liu, and Xinggang Wang. Densely connected search space for more flexible neural architecture search. In *CVPR*, pages 10628–10637, 2020. 1
- [30] Andreas Geiger, Philip Lenz, and Raquel Urtasun. Are we ready for autonomous driving? the kitti vision benchmark suite. In *CVPR*, pages 3354–3361, 2012. 6, 9
- [31] Golnaz Ghiasi, Tsung-Yi Lin, and Quoc V Le. Nas-fpn: Learning scalable feature pyramid architecture for object detection. In *CVPR*, pages 7036–7045, 2019. 3
- [32] Xinyu Gong, Wuyang Chen, Yifan Jiang, Ye Yuan, Xianming Liu, Qian Zhang, Yuan Li, and Zhangyang Wang. Autopose: Searching multi-scale branch aggregation for pose estimation. *arXiv preprint arXiv:2008.07018*, 2020. 3, 7
- [33] Ronghao Guo, Chen Lin, Chuming Li, Keyu Tian, Ming Sun, Lu Sheng, and Junjie Yan. Powering one-shot topological nas with stabilized share-parameter proxy. In *ECCV*, 2020. 6
- [34] Zichao Guo, Xiangyu Zhang, Haoyuan Mu, Wen Heng, Zechun Liu, Yichen Wei, and Jian Sun. Single path one-shot neural architecture search with uniform sampling. In *ECCV*, 2020. 3, 6
- [35] Kaiming He, Xiangyu Zhang, Shaoqing Ren, and Jian Sun. Deep residual learning for image recognition. In *CVPR*, pages 770–778, 2016. 4
- [36] Andrew Howard, Mark Sandler, Grace Chu, Liang-Chieh Chen, Bo Chen, Mingxing Tan, Weijun Wang, Yukun Zhu, Ruoming Pang, Vijay Vasudevan, et al. Searching for mobilenetv3. In *ICCV*, pages 1314–1324, 2019. 3, 6, 7
- [37] Jie Hu, Li Shen, and Gang Sun. Squeeze-and-excitation networks. In *CVPR*, pages 7132–7141, 2018. 2, 9, 10, 11
- [38] Yibo Hu, Xiang Wu, and Ran He. Tf-nas: Rethinking three search freedoms of latency-constrained differentiable neural architecture search. In *ECCV*, 2020. 6
- [39] Gao Huang, Shichen Liu, Laurens Van der Maaten, and Kilian Q Weinberger. Condensenet: An efficient densenet using learned group convolutions. In *CVPR*, pages 2752–2761, 2018. 6
- [40] Xiaoqi Jiao, Yichun Yin, Lifeng Shang, Xin Jiang, Xiao Chen, Linlin Li, Fang Wang, and Qun Liu. Tinybert: Distill-

- ing bert for natural language understanding. *arXiv preprint arXiv:1909.10351*, 2019. 2
- [41] Xiaojie Jin, Jiang Wang, Joshua Slocum, Ming-Hsuan Yang, Shengyang Dai, Shuicheng Yan, and Jiashi Feng. Rc-darts: Resource constrained differentiable architecture search. *arXiv preprint arXiv:1912.12814*, 2019. 3
- [42] Alexander Kirillov, Yuxin Wu, Kaiming He, and Ross Girshick. Pointrend: Image segmentation as rendering. In *CVPR*, pages 9799–9808, 2020. 2
- [43] Alex H Lang, Sourabh Vora, Holger Caesar, Lubing Zhou, Jiong Yang, and Oscar Beijbom. Pointpillars: Fast encoders for object detection from point clouds. In *CVPR*, pages 12697–12705, 2019. 7, 9, 10
- [44] Hanchao Li, Pengfei Xiong, Haoqiang Fan, and Jian Sun. Dfanet: Deep feature aggregation for real-time semantic segmentation. In *CVPR*, pages 9522–9531, 2019. 2, 6, 7
- [45] Liam Li and Ameet Talwalkar. Random search and reproducibility for neural architecture search. In *Uncertainty in Artificial Intelligence*, pages 367–377. PMLR, 2020. 6, 7
- [46] Hanwen Liang, Shifeng Zhang, Jiacheng Sun, Xingqiu He, Weiran Huang, Kechen Zhuang, and Zhenguo Li. Darts+: Improved differentiable architecture search with early stopping. *arXiv preprint arXiv:1909.06035*, 2019. 1
- [47] Peiwen Lin, Peng Sun, Guangliang Cheng, Sirui Xie, Xi Li, and Jianping Shi. Graph-guided architecture search for real-time semantic segmentation. In *CVPR*, pages 4203–4212, 2020. 1, 3, 6, 7
- [48] Tsung-Yi Lin, Michael Maire, Serge Belongie, James Hays, Pietro Perona, Deva Ramanan, Piotr Dollár, and C Lawrence Zitnick. Microsoft coco: Common objects in context. In *ECCV*, pages 740–755. Springer, 2014. 6, 9
- [49] Chenxi Liu, Liang-Chieh Chen, Florian Schroff, Hartwig Adam, Wei Hua, Alan L Yuille, and Li Fei-Fei. Auto-deeplab: Hierarchical neural architecture search for semantic image segmentation. In *CVPR*, pages 82–92, 2019. 1, 2, 3, 6, 7
- [50] Hanxiao Liu, Karen Simonyan, and Yiming Yang. DARTS: differentiable architecture search. In *ICLR*, 2019. 1, 3, 5
- [51] Weijie Liu, Peng Zhou, Zhe Zhao, Zhiruo Wang, Haotang Deng, and Qi Ju. Fastbert: a self-distilling bert with adaptive inference time. *arXiv preprint arXiv:2004.02178*, 2020. 2
- [52] Zhuang Liu, Jianguo Li, Zhiqiang Shen, Gao Huang, Shoumeng Yan, and Changshui Zhang. Learning efficient convolutional networks through network slimming. In *ICCV*, pages 2736–2744, 2017. 5
- [53] Shao-Yuan Lo, Hsueh-Ming Hang, Sheng-Wei Chan, and Jing-Jhih Lin. Efficient dense modules of asymmetric convolution for real-time semantic segmentation. In *Proceedings of the ACM Multimedia Asia*, pages 1–6, 2019. 7
- [54] Zhichao Lu, Ian Whalen, Vishnu Boddeti, Yashesh Dhebar, Kalyanmoy Deb, Erik Goodman, and Wolfgang Banzhaf. Nsga-net: A multi-objective genetic algorithm for neural architecture search. *arXiv preprint arXiv:1810.03522*, 2018. 3
- [55] Ningning Ma, Xiangyu Zhang, Hai-Tao Zheng, and Jian Sun. Shufflenet v2: Practical guidelines for efficient cnn architecture design. In *ECCV*, pages 116–131, 2018. 6, 7, 8
- [56] Jieru Mei, Yingwei Li, Xiaochen Lian, Xiaojie Jin, Linjie Yang, Alan Yuille, and Jianchao Yang. Atomnas: Fine-grained end-to-end neural architecture search. In *ICLR*, 2020. 1, 3, 5, 6, 9
- [57] Vladimir Nekrasov, Hao Chen, Chunhua Shen, and Ian Reid. Fast neural architecture search of compact semantic segmentation models via auxiliary cells. In *CVPR*, pages 9126–9135, 2019. 1, 3, 7
- [58] Marin Orsic, Ivan Kreso, Petra Bevandic, and Sinisa Segvic. In defense of pre-trained imagenet architectures for real-time semantic segmentation of road-driving images. In *CVPR*, pages 12607–12616, 2019. 7
- [59] Hyojin Park, Youngjoon Yoo, Geonseok Seo, Dongyoon Han, Sangdoo Yun, and Nojun Kwak. C3: Concentrated-comprehensive convolution and its application to semantic segmentation. *arXiv preprint arXiv:1812.04920*, 2018. 7
- [60] Adam Paszke, Abhishek Chaurasia, Sangpil Kim, and Eugenio Culurciello. Enet: A deep neural network architecture for real-time semantic segmentation. *arXiv preprint arXiv:1606.02147*, 2016. 7
- [61] Alec Radford, Karthik Narasimhan, Tim Salimans, and Ilya Sutskever. Improving language understanding by generative pre-training, 2018. 2
- [62] Prajit Ramachandran, Barret Zoph, and Quoc V Le. Searching for activation functions. *arXiv preprint arXiv:1710.05941*, 2017. 6, 9
- [63] Esteban Real, Sherry Moore, Andrew Selle, Saurabh Saxena, Yutaka Leon Suematsu, Jie Tan, Quoc Le, and Alex Kurakin. Large-scale evolution of image classifiers. *arXiv preprint arXiv:1703.01041*, 2017. 3
- [64] Xingkai Ren, Ronghua Shi, and Fangfang Li. Distill bert to traditional models in chinese machine reading comprehension. In *AAAI*, pages 13901–13902, 2020. 2
- [65] Mark Sandler, Andrew Howard, Menglong Zhu, Andrey Zhmoginov, and Liang-Chieh Chen. Mobilenetv2: Inverted residuals and linear bottlenecks. In *CVPR*, pages 4510–4520, 2018. 3, 6, 7, 8
- [66] Albert Shaw, Daniel Hunter, Forrest Landola, and Sammy Sidhu. Squeezeenas: Fast neural architecture search for faster semantic segmentation. In *ICCVW*, 2019. 1, 3, 7
- [67] Albert Shaw, Wei Wei, Weiyang Liu, Le Song, and Bo Dai. Meta architecture search. In *NeurIPS*, pages 11227–11237, 2019. 1
- [68] Mennatullah Siam, Mostafa Gamal, Moemen Abdel-Razek, Senthil Yogamani, and Martin Jagersand. Rtseg: Real-time semantic segmentation comparative study. In *ICIP*, pages 1603–1607. IEEE, 2018. 7
- [69] David R So, Chen Liang, and Quoc V Le. The evolved transformer. *arXiv preprint arXiv:1901.11117*, 2019. 2
- [70] Dimitrios Stamoulis, Ruizhou Ding, Di Wang, Dimitrios Lymberopoulos, Bodhi Priyantha, Jie Liu, and Diana Marculescu. Single-path nas: Designing hardware-efficient convnets in less than 4 hours. In *ECML-PKDD*, pages 481–497. Springer, 2019. 3, 9
- [71] Mingxing Tan, Bo Chen, Ruoming Pang, Vijay Vasudevan, Mark Sandler, Andrew Howard, and Quoc V Le. Mnasnet: Platform-aware neural architecture search for mobile. In *CVPR*, pages 2820–2828, 2019. 3, 6, 9

- [72] Mingxing Tan and Quoc V. Le. Efficientnet: Rethinking model scaling for convolutional neural networks. In *ICML*, pages 6105–6114, 2019. 6, 9
- [73] Mingxing Tan and Quoc V. Le. Mixconv: Mixed depthwise convolutional kernels. *arXiv preprint arXiv:1907.09595*, 2019. 3, 5, 6
- [74] Sercan Türkmen and Janne Heikkilä. An efficient solution for semantic segmentation: Shufflenet v2 with atrous separable convolutions. In *Scandinavian Conference on Image Analysis*, pages 41–53. Springer, 2019. 7
- [75] Ashish Vaswani, Noam Shazeer, Niki Parmar, Jakob Uszkoreit, Llion Jones, Aidan N Gomez, Łukasz Kaiser, and Illia Polosukhin. Attention is all you need. In *NeurIPS*, pages 5998–6008, 2017. 2, 3, 4, 7
- [76] Jingdong Wang, Ke Sun, Tianheng Cheng, Borui Jiang, Chaorui Deng, Yang Zhao, Dong Liu, Yadong Mu, Mingkui Tan, Xinggang Wang, et al. Deep high-resolution representation learning for visual recognition. *IEEE TPAMI*, 2020. 1, 2, 4, 7, 9
- [77] Sinong Wang, Belinda Li, Madian Khabsa, Han Fang, and Hao Ma. Linformer: Self-attention with linear complexity. *arXiv preprint arXiv:2006.04768*, 2020. 2
- [78] Xiaolong Wang, Ross Girshick, Abhinav Gupta, and Kaiming He. Non-local neural networks. In *CVPR*, pages 7794–7803, 2018. 2, 10, 11
- [79] Bichen Wu, Xiaoliang Dai, Peizhao Zhang, Yanghan Wang, Fei Sun, Yiming Wu, Yuandong Tian, Peter Vajda, Yangqing Jia, and Kurt Keutzer. Fbnets: Hardware-aware efficient convnet design via differentiable neural architecture search. In *CVPR*, pages 10734–10742, 2019. 1, 6
- [80] Bichen Wu, Chenfeng Xu, Xiaoliang Dai, Alvin Wan, Peizhao Zhang, Masayoshi Tomizuka, Kurt Keutzer, and Peter Vajda. Visual transformers: Token-based image representation and processing for computer vision. *arXiv preprint arXiv:2006.03677*, 2020. 2
- [81] Bin Xiao, Haiping Wu, and Yichen Wei. Simple baselines for human pose estimation and tracking. In *ECCV*, pages 466–481, 2018. 7
- [82] Sirui Xie, Hehui Zheng, Chunxiao Liu, and Liang Lin. Snas: stochastic neural architecture search. *arXiv preprint arXiv:1812.09926*, 2018. 1
- [83] Yuhui Xu, Lingxi Xie, Xiaopeng Zhang, Xin Chen, Guo-Jun Qi, Qi Tian, and Hongkai Xiong. Pcdarts: Partial channel connections for memory-efficient differentiable architecture search. *arXiv preprint arXiv:1907.05737*, 2019. 3
- [84] Sen Yang, Wankou Yang, and Zhen Cui. Pose neural fabrics search. *arXiv preprint arXiv:1909.07068*, 2019. 7
- [85] Shan You, Tao Huang, Mingmin Yang, Fei Wang, Chen Qian, and Changshui Zhang. Greedynas: Towards fast one-shot nas with greedy supernet. In *CVPR*, pages 1999–2008, 2020. 9
- [86] Changqian Yu, Jingbo Wang, Chao Peng, Changxin Gao, Gang Yu, and Nong Sang. Bisenet: Bilateral segmentation network for real-time semantic segmentation. In *ECCV*, pages 325–341, 2018. 7
- [87] Jiahui Yu and Thomas Huang. Autoslim: Towards one-shot architecture search for channel numbers. *arXiv preprint arXiv:1903.11728*, 2019. 6
- [88] Jiahui Yu, Pengchong Jin, Hanxiao Liu, Gabriel Bender, Pieter-Jan Kindermans, Mingxing Tan, Thomas Huang, Xiaodan Song, Ruoming Pang, and Quoc Le. Bignas: Scaling up neural architecture search with big single-stage models. In *ECCV*, 2020. 3, 6
- [89] Jiahui Yu, Linjie Yang, Ning Xu, Jianchao Yang, and Thomas Huang. Slimmable neural networks. *arXiv preprint arXiv:1812.08928*, 2018. 5
- [90] Hongyi Zhang, Moustapha Cisse, Yann N Dauphin, and David Lopez-Paz. mixup: Beyond empirical risk minimization. *arXiv preprint arXiv:1710.09412*, 2017. 6
- [91] Hang Zhang, Kristin Dana, Jianping Shi, Zhongyue Zhang, Xiaogang Wang, Ambrish Tyagi, and Amit Agrawal. Context encoding for semantic segmentation. In *CVPR*, pages 7151–7160, 2018. 1
- [92] Xiong Zhang, Hongmin Xu, Hong Mo, Jianchao Tan, Cheng Yang, and Wenqi Ren. Dcnas: Densely connected neural architecture search for semantic image segmentation. *arXiv preprint arXiv:2003.11883*, 2020. 2, 3
- [93] Xiangyu Zhang, Xinyu Zhou, Mengxiao Lin, and Jian Sun. Shufflenet: An extremely efficient convolutional neural network for mobile devices. In *CVPR*, pages 6848–6856, 2018. 6, 7
- [94] Hengshuang Zhao, Jianping Shi, Xiaojuan Qi, Xiaogang Wang, and Jiaya Jia. Pyramid scene parsing network. In *CVPR*, pages 2881–2890, 2017. 8
- [95] Bolei Zhou, Hang Zhao, Xavier Puig, Sanja Fidler, Adela Barriuso, and Antonio Torralba. Scene parsing through ade20k dataset. In *CVPR*, pages 633–641, 2017. 6, 9
- [96] Yanqi Zhou, Peng Wang, Sercan Arik, Haonan Yu, Syed Zawad, Feng Yan, and Greg Diamos. Epnas: Efficient progressive neural architecture search. *BMVC*, 2019. 1
- [97] Barret Zoph and Quoc V. Le. Neural architecture search with reinforcement learning. In *ICLR*, 2017. 2